npj climate and atmospheric science

Supplementary information for "The role of upper-ocean variations of the Kuroshio-Oyashio Extension in seasonal-to-decadal air-sea heat flux variability "

Youngji Joh[1], Thomas L. Delworth[2], Andrew T. Wittenberg[2], Xiaosong Yang[2], Anthony Rosati[2,3], Nathaniel C. Johnson[2], and Liwei Jia[2,3]

[1] *Atmospheric and Oceanic Sciences Program, Princeton University, Princeton, NJ, USA*

[2] *Geophysical Fluid Dynamics Laboratory/NOAA, 201 Forrestal Road, Princeton, NJ, USA*

[3] *University Corporation for Atmospheric Research, Boulder, CO, USA*

*Corresponding author: Youngji Joh (youngji.joh@princeton.edu)

Contents of this file

Supplementary Figures 1 to 10

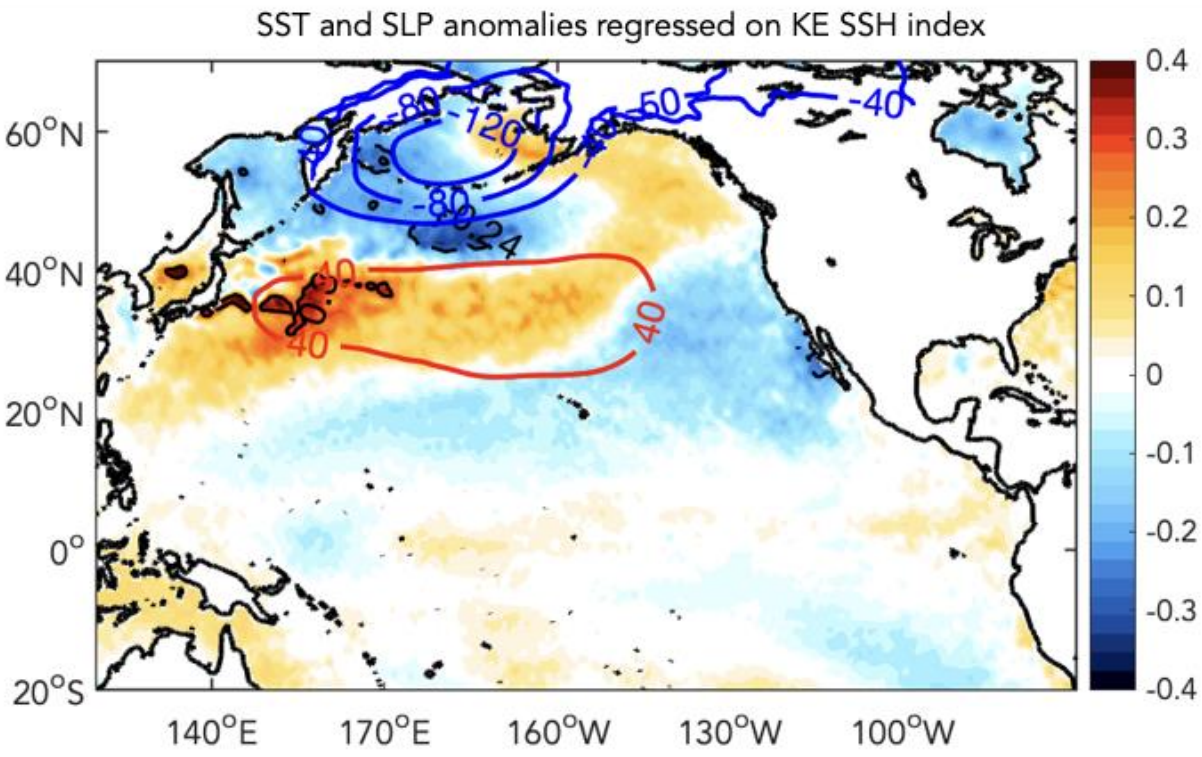

Supplementary Figure 1. Zoomed-out distribution of SST and SLP associated with KE SSH. Map of regression coefficient of SST (shading; °C) and SLP (contour; Pa) anomalies with the normalized KE SSH index. Contours denote SST (black) and SLP (blue and red) regression coefficients that are statistically significant at the 10% level.

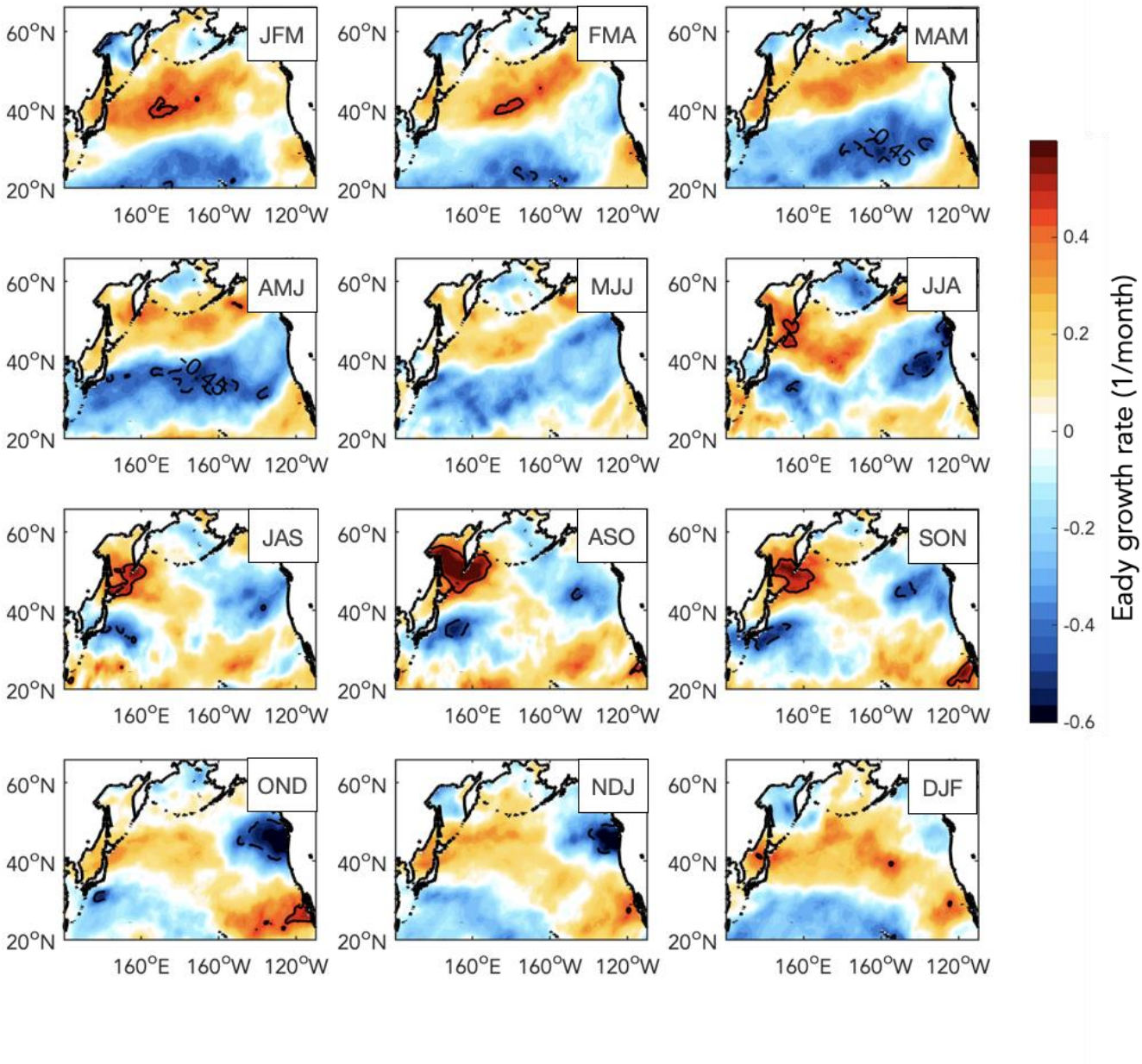

Supplementary Figure 2. Seasonal maximum Eady growth rate associated with KE SSH. a, Spatial maps of regression coefficients for the linear regression of the maximum Eady growth rate anomalies on the normalized KE SSH index without lags. Following Lindzen and Farrell (1980), the Eady growth rate is defined as the magnitude of the baroclinicity $|\sigma_{BI}| = 0.31\,(\frac{f}{N})\frac{\partial|\boldsymbol{u}|}{\partial z}$ with $N = \left(\frac{g}{\theta}\frac{\partial\theta}{\partial z}\right)^{1/2}$, where f is Coriolis parameter, N is buoyancy coefficient, g is gravitational acceleration, θ is potential temperature, z is height, and $|\mathbf{u}|$ is the magnitude of horizontal wind speed. The discretized form used here represents the atmospheric layer between 850 and 500hPa. Contours denote regression coefficients that are statistically significant at the 10% level.

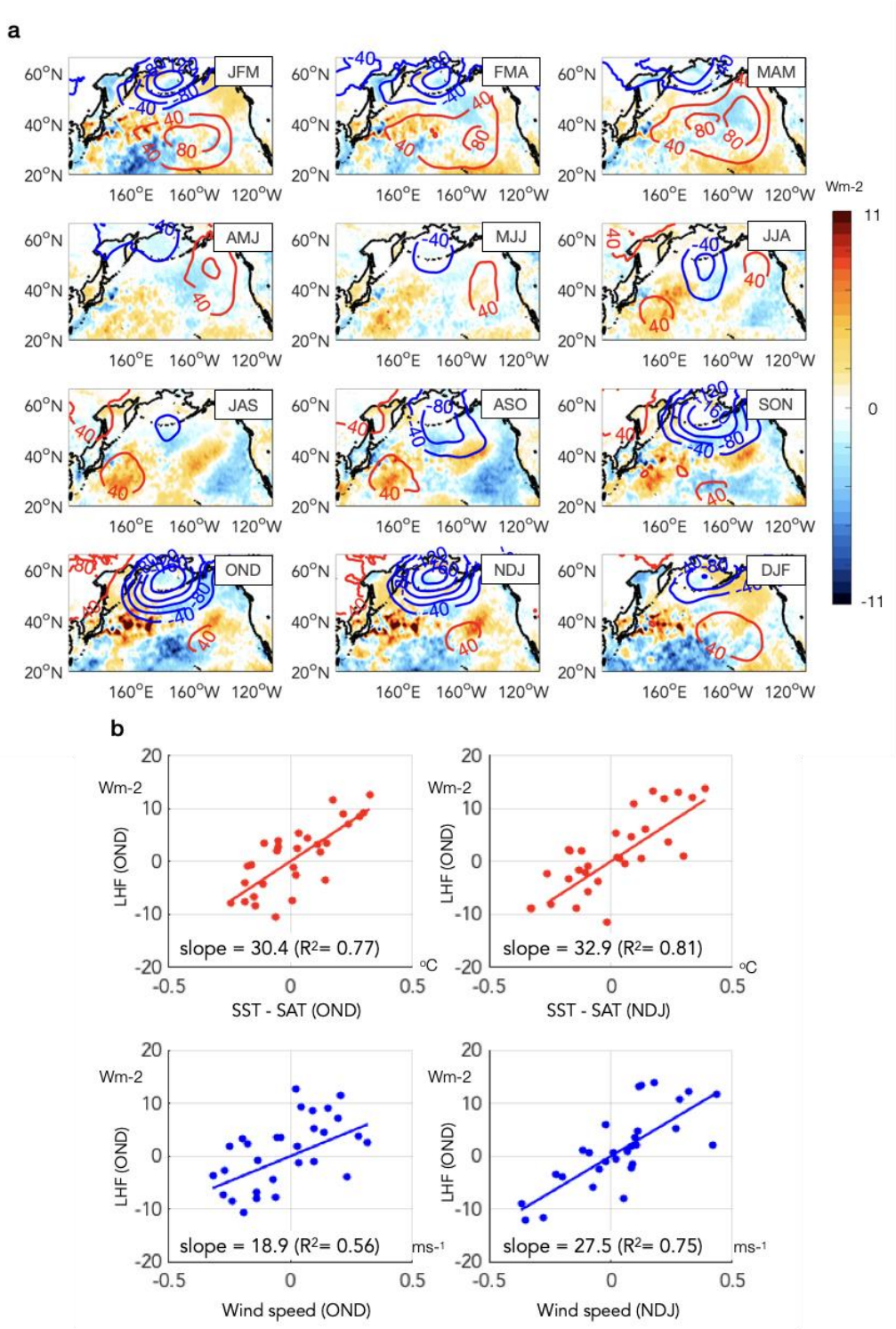

Supplementary Figure 3. Seasonal air-sea coupled patterns associated with KE SSH and quantification of KOE LHF anomalies. a, Spatial maps of regression coefficients for the linear regression of surface LHF (shading; Wm-2) and SLP (contours; Pa) anomalies on the normalized KE SSH index without lags. **b**, Scatterplots of areal indices between LHF vs. sea-air temperature difference (SST-SAT; ^{o}C) in the top panels and LHF vs. wind speed (ms^{-1}) anomalies in the bottom panels over the KOE region (25^{o}-45^{o}N & 135^{o}-180^{o}E). OND (left panels) and NDJ (right panel) time series are used. The straight lines are least squares linear fits to the scatter points; regression coefficient (slope), and squared correlation coefficient (r^2) are shown in each plot.

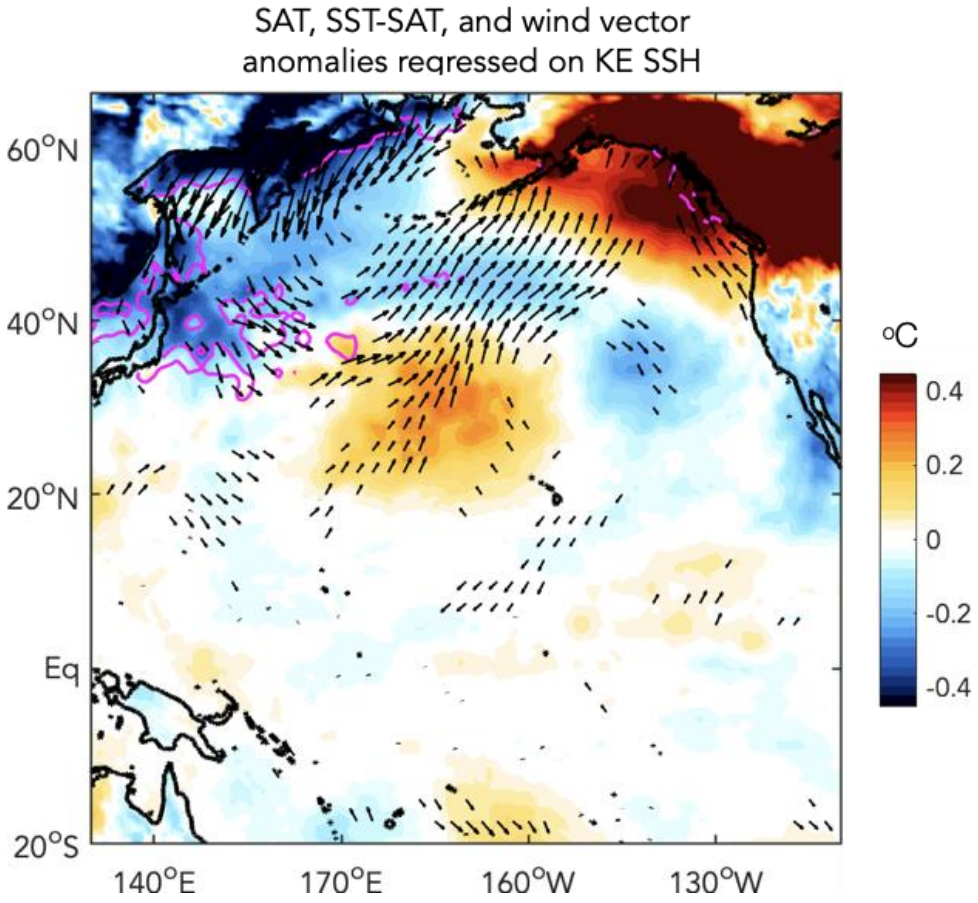

Supplementary Figure 4. Insignificant contributions of air temperature anomalies to boreal winter KOE surface heat exchange. Regression coefficients for the linear regression of NDJ SAT (shading; °C), SST-SAT (contour; °C), and wind vector (m/s) anomalies on the AOS KE SSH index (normalized).

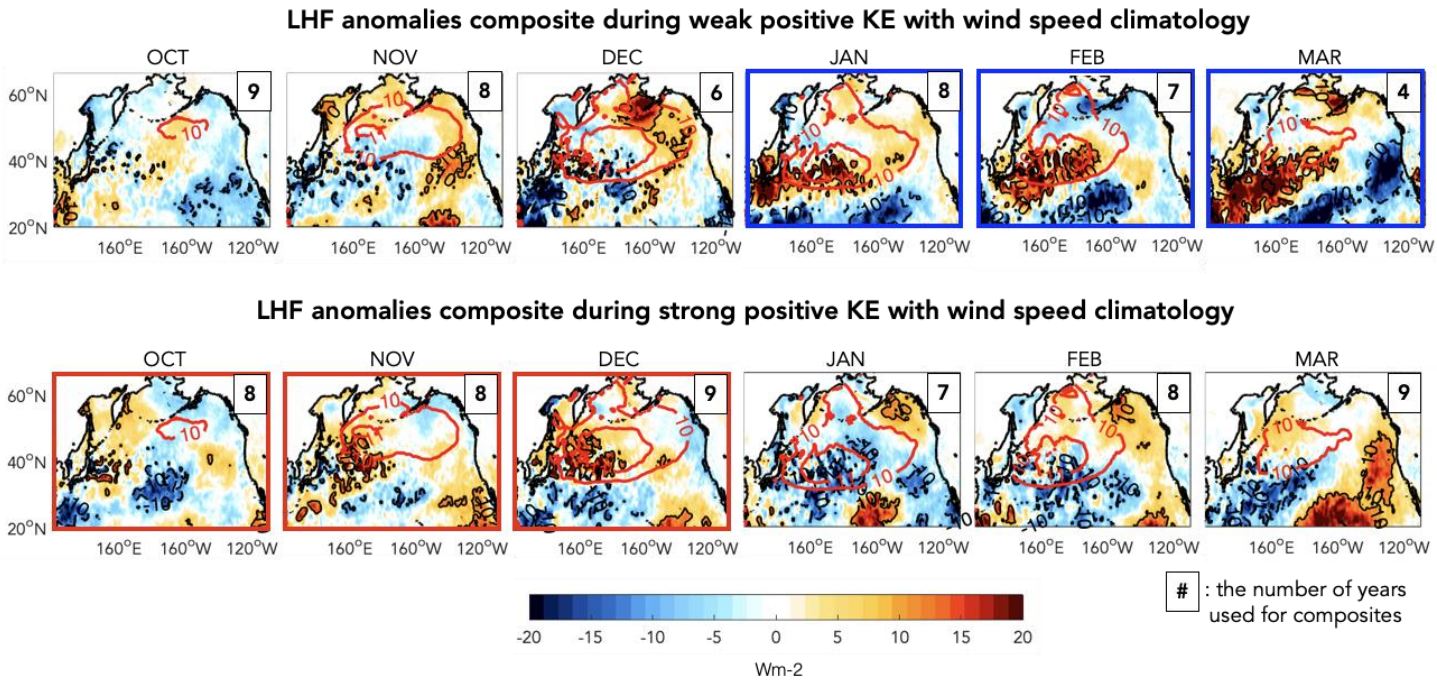

Supplementary Figure 5. A comparison of seasonal changes in LHF anomalies associated with KE SSH between strong and weak positive KE phase. Composites of LHF anomalies (shadings; Wm-2) for events positive, but below (upper) and exceeding (bottom) 0.7 standard deviation of the positive KE SSH, overlaid with monthly long-term mean of wind speed (red contours; m/s). The number of years used in composites are indicated in the small box in the top-right corner in each panel.

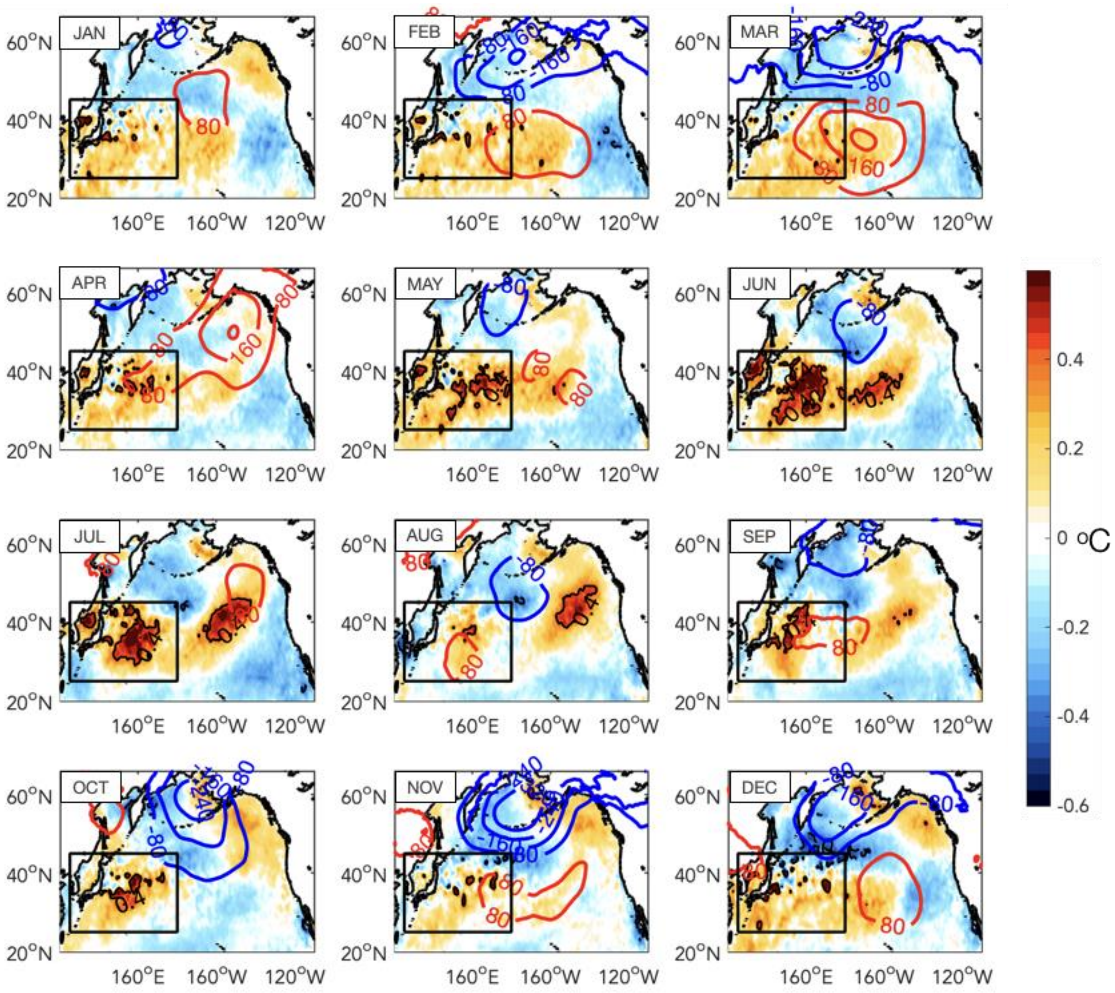

Supplementary Figure 6. Monthly air-sea coupled anomalies associated with KE SSH. Spatial maps of regression coefficients for the linear regression of surface LHF (shading; Wm-2) and SLP (contours; Pa) anomalies on the normalized KE SSH index without lags. Monthly LHF anomalies and KE SSH index are used.

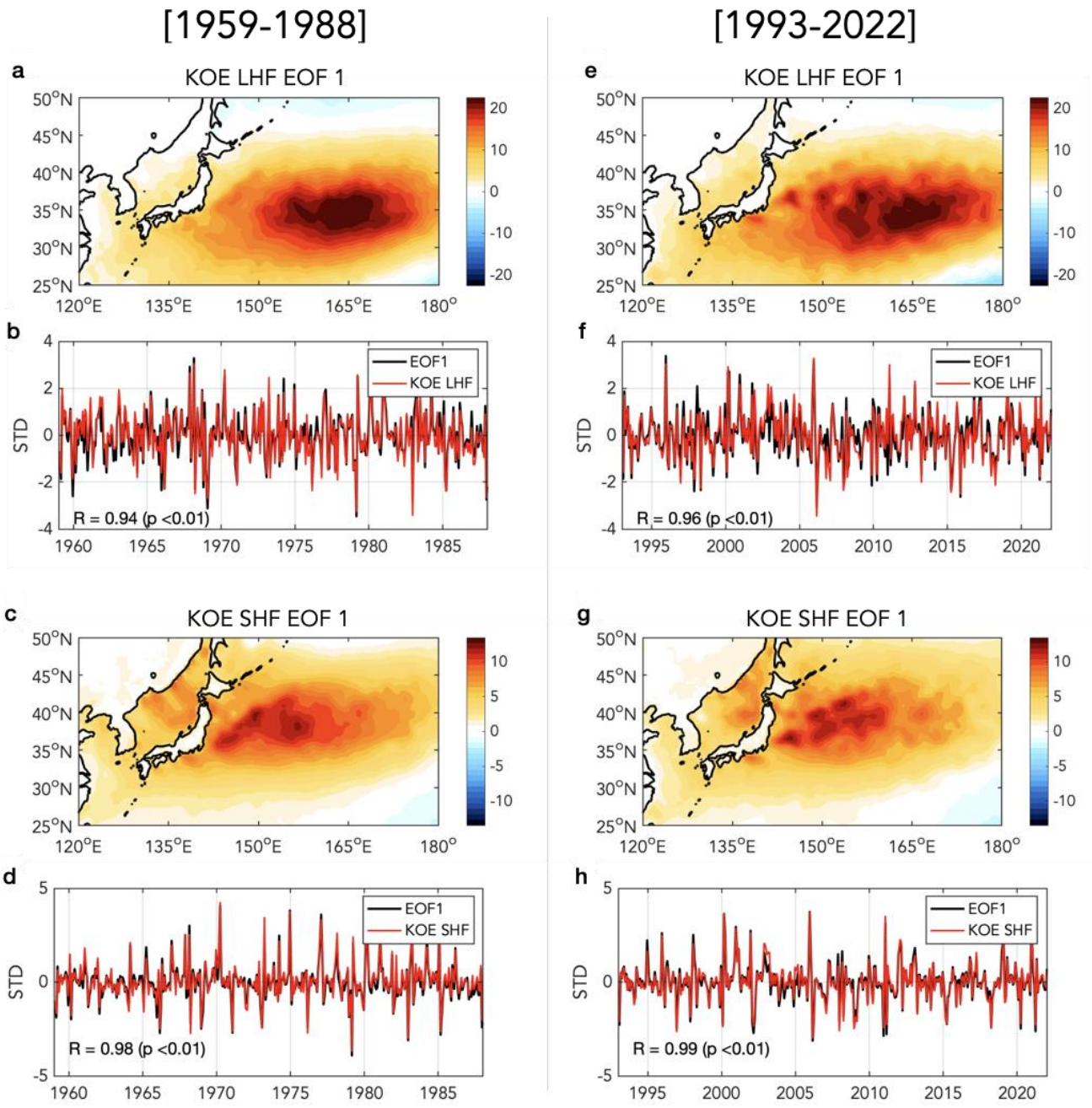

Supplementary Figure 7. KOE heat flux variations over the observational record. a-b, LHF anomalies (a) regressed on the leading Principal component (PC) time series (b) obtained from empirical orthogonal faction (EOF) of KOE (30°-45°N & 140°-170°E) LHF monthly anomalies for the years 1959-1988. In b, the first mode of EOF time series (black) shows that the KOE LHF index (red) defined in this study effectively captures the most dominant heat flux variability over the KOE region. **c-d,** Same as in (a-b) but for the SHF. **e-h**, Same as in (a-d) but for the years 1993-2022.

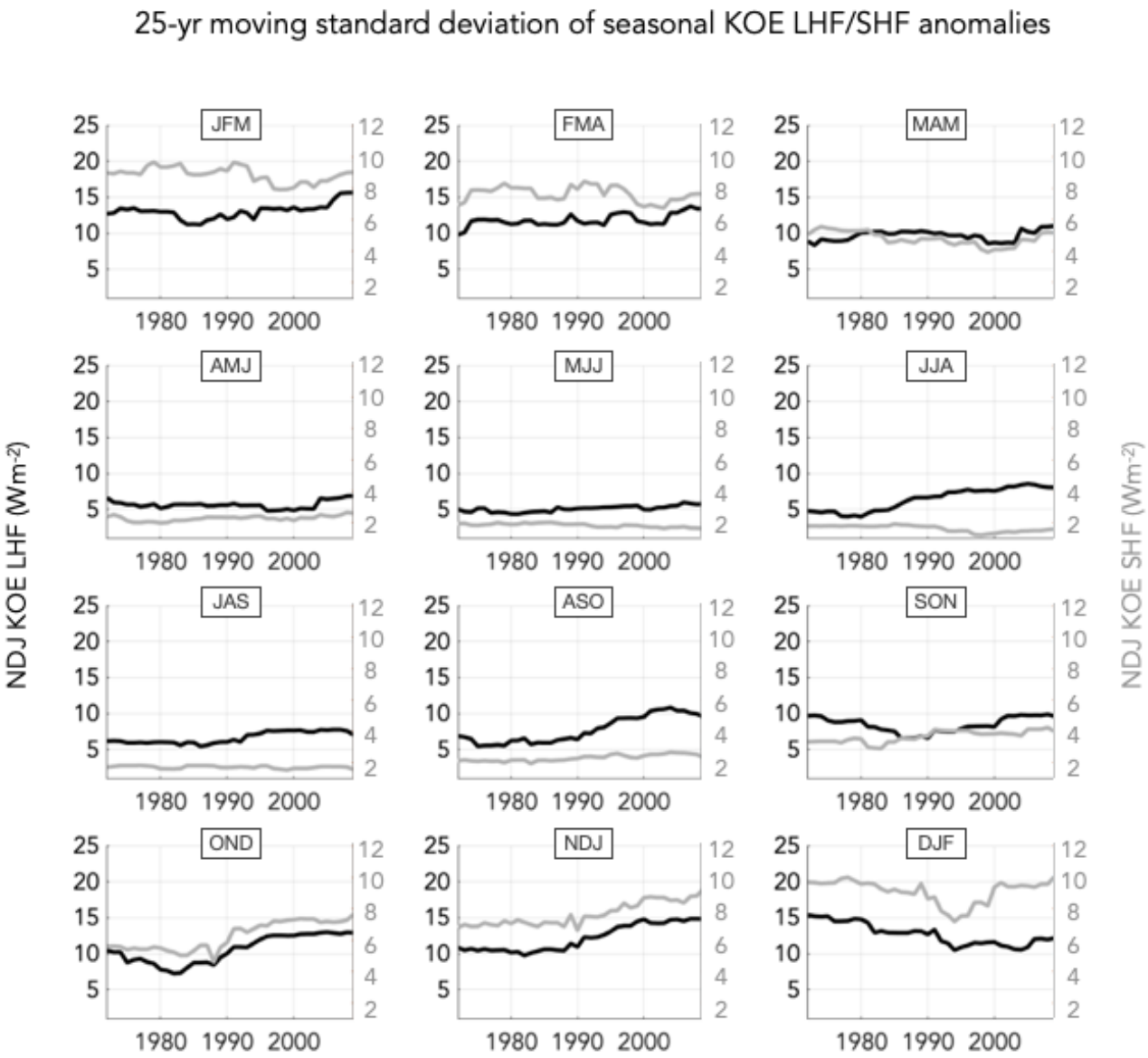

Supplementary Figure 8. 25-year moving standard deviation of seasonal NDJ KOE LHF (black) and SHF (gray) indices for the period between 1959-2021. The moving windows are computed with increments of one year.

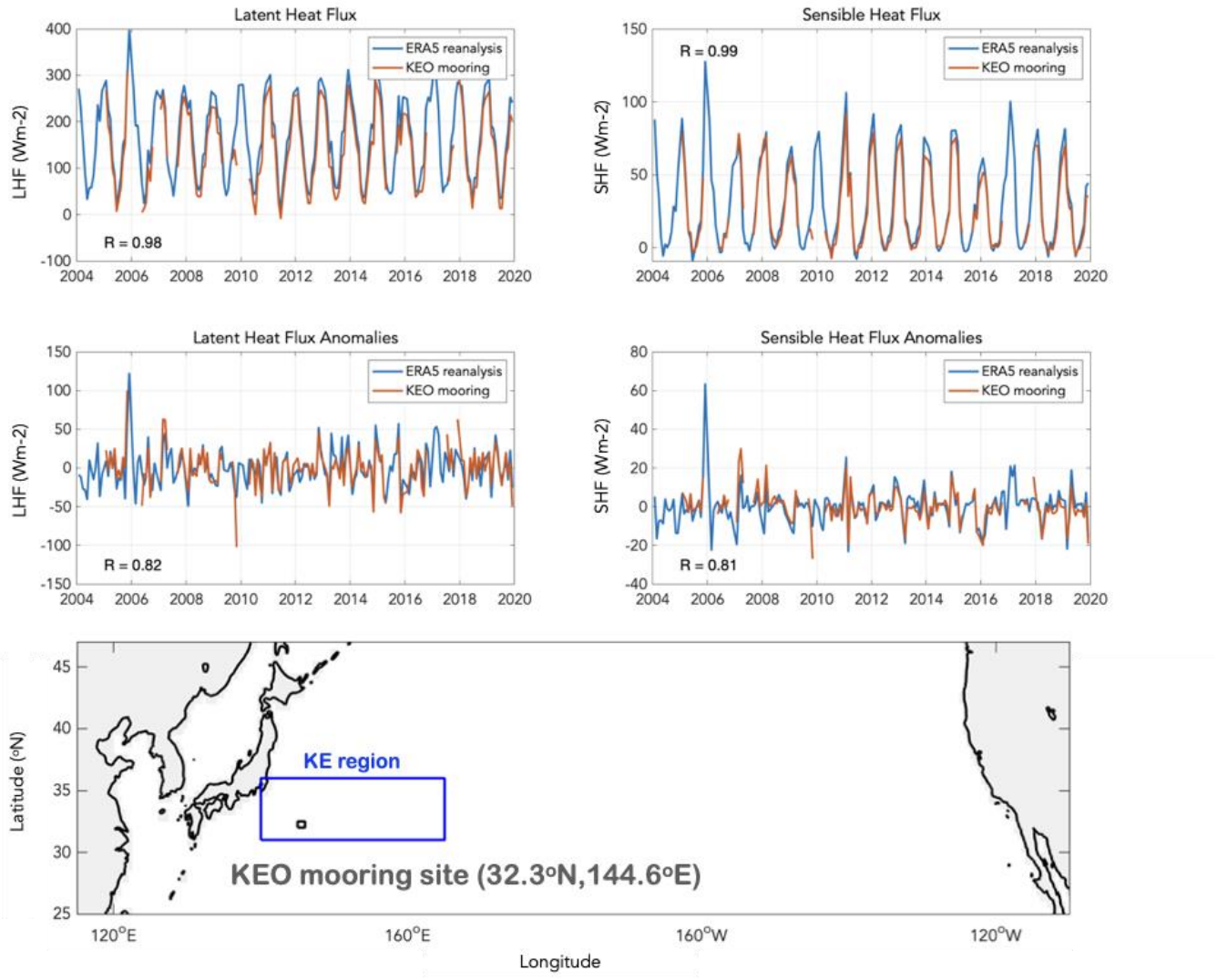

Supplementary Figure 9. Time series of LHF and SHF at KEO mooring site (32.3°N & 144.6°E) and the mooring location. LHF and SHF data from observational reanalysis (ERA5) are compared with in situ mooring data of Kuroshio Extension Observatory (KEO) from Ocean Climate Stations project. The daily mooring data between is used for the period between 2004-2020. The KEO mooring site and the KE region are indicated in the bottom panel.

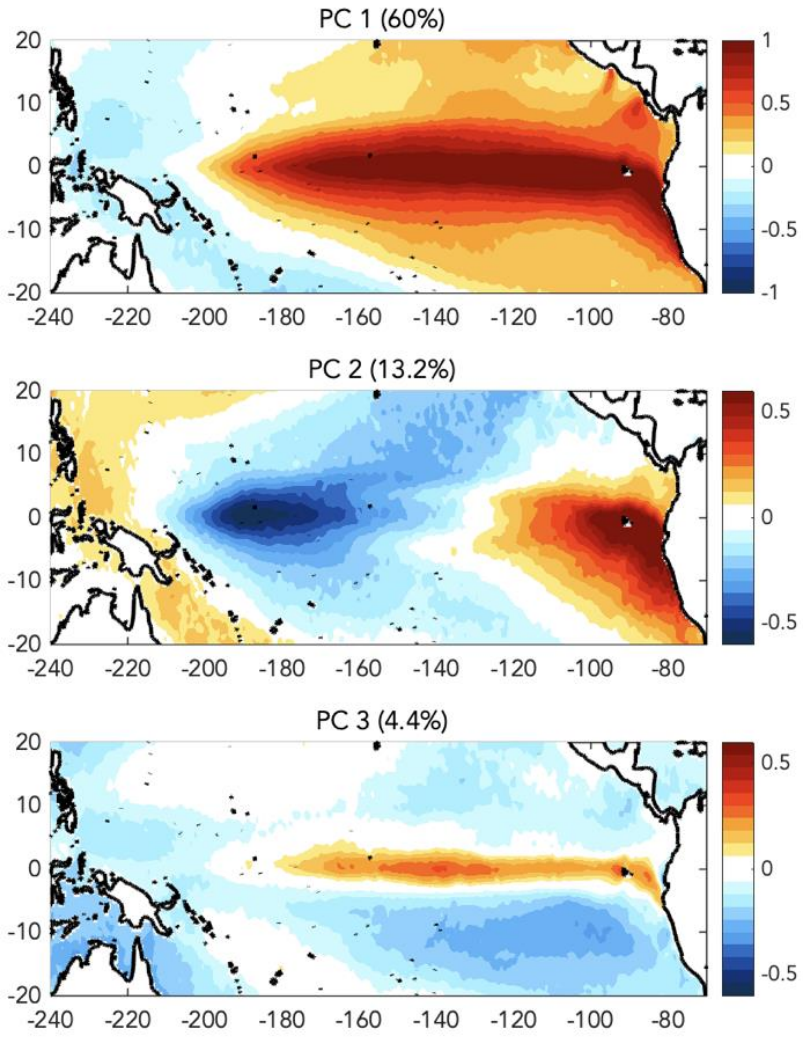

Supplementary Figure 10. ENSO patterns used in removal of tropical SST variations from midlatitude Pacific. Regression coefficient of the tropical Pacific SST onto the (top) first, (middle) second, and (bottom) third PCs, which are obtained from SST EOF over the tropical Pacific (120°E-80°W & 12.5°S and 12.5°N).